

Neural net modeling of equilibria in NSTX-U

J.T. Wai^a, M.D. Boyer^b, E. Kolemen^{a,b,*}

^a*Princeton University, Princeton, New Jersey, USA*

^b*Princeton Plasma Physics Laboratory, Princeton, New Jersey, USA*

Abstract

Neural networks (NNs) offer a path towards synthesizing and interpreting data on faster timescales than traditional physics-informed computational models. In this work we develop two neural networks relevant to equilibrium and shape control modeling, which are part of a suite of tools being developed for the National Spherical Torus Experiment-Upgrade (NSTX-U) for fast prediction, optimization, and visualization of plasma scenarios. The networks include *Eqnet*, a free-boundary equilibrium solver trained on the EFIT01 reconstruction algorithm, and *Pertnet*, which is trained on the Gspert code and predicts the non-rigid plasma response, a nonlinear term that arises in shape control modeling. The equilibrium neural network is trained with different combinations of inputs and outputs in order to offer flexibility in use cases. In particular, the NN can use magnetic diagnostics as inputs for equilibrium prediction thus acting as a reconstruction code, or can use profiles and external currents as inputs to act as a traditional free-boundary Grad-Shafranov solver. We report strong performance for both networks indicating that these models could reliably be used within closed-loop simulations. Some limitations regarding generalizability and noise are discussed.

Keywords: neural net, equilibrium, shape control

1. Introduction

In tokamaks, a critical aspect of achieving high performance plasma operation and maximizing scientific exploration is the development of fast and reliable model predictions of the plasma behavior. Fast model predictions are often a prerequisite to implementing real-time control algorithms. Additionally, if these are not available in real-time, but on a slightly slower timescale, they can be used by physics operators to inform decisions between shots. Machine learning is a tool that is gaining increasing usage in the nuclear fusion community and can be useful in this type of situation where it is desirable to quickly synthesize data into interpretable outputs. Some examples include its usage in profile predictions [1–3], turbulent transport [4], identifying scalings laws [5, 6], and predicting instabilities and disruptions [7–13].

In this work, we present two neural nets (NNs) *Eqnet* and *Pertnet* developed for the NSTX-U tokamak which are relevant to equilibrium and shape control modeling. Along with recent modeling of neutral beam heating [14] and electron profiles [3], these neural nets are part of a suite of tools being developed for fast prediction, optimization, and visualization of plasma scenarios. Closed-loop simulations of a plasma discharge are generally too slow for usage between shots due to time-intensive steps of repeatedly solving the free-boundary Grad-Shafranov equation

and linearizing around the given equilibrium. The neural nets here were developed to perform these two time-intensive tasks as a step towards fast simulation and eventually, numerical optimization of scenarios. Additionally, we explore and report on additional modes of operation of the networks that may have alternative uses.

Section 2 introduces *Eqnet*, a neural net trained to predict the free-boundary plasma equilibrium based on various sets of inputs. In this work, we distinguish between several modes of operation (forward, forward-control, reconstruction, reconstruction-control) as diagrammed in fig. 1. The *forward* mode predicts the equilibrium flux surfaces using the coil currents and plasma profiles as inputs. In contrast the *forward-control* mode directly predicts control-relevant shaping parameters that are normally derived from the flux surfaces, including quantities such as the x-point locations, elongation, and outer gap distance. Similarly the *reconstruction* and *reconstruction-control* modes predict the same outputs, but use diagnostic information such as magnetic probes as inputs to the NN. Previous neural net equilibrium solvers [15–22] were developed in the spirit of reconstruction-control mode—mapping diagnostics to shaping parameters—with some exceptions such as [23] which reconstructs flux surfaces and [24] which is a fixed-boundary solver. Similar to previous efforts on other machines, we obtain good predictions using the magnetic diagnostics. However, our primary focus is on the forward mode for its usage as a fast free-boundary Grad-Shafranov solver which is more applicable to the simulation goals above.

*Corresponding author

Email addresses: jwai@princeton.edu (J.T. Wai),
ekolemen@princeton.edu (E. Kolemen)

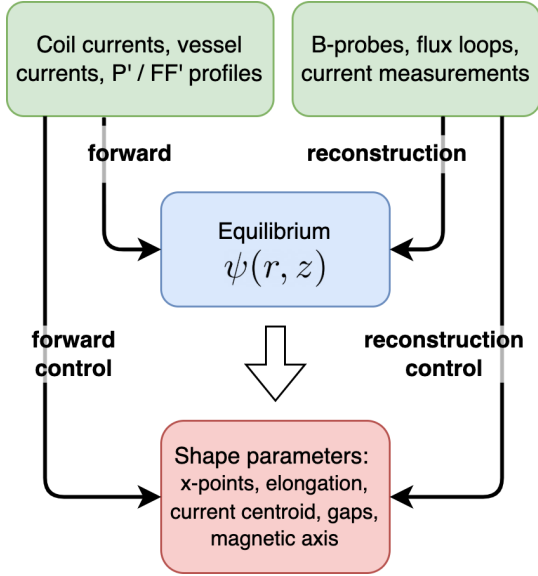


Figure 1: Diagram of the data inputs and outputs that were used to train different versions of Eqnet. The forward modes solve eq. (1) directly whereas the reconstruction modes are a diagnostic best-fit solution. The control modes predict extracted shaping parameters instead of the flux surfaces.

For control simulations, another important calculation is ‘linearizing the equilibrium’ which includes obtaining the non-rigid plasma response, how current in the plasma shifts and redistributes in response to applied fields from the poloidal field (PF) coils. It is also common to model the plasma response to the normalized internal inductance l_i and plasma poloidal beta β_p . This effect is nonlinear, equilibrium-dependent, and is addressed by codes such as Gspert/Gsupdate [25, 26] and Create-L/NL [27, 28]. We introduce Pertnet, a neural net for identifying the plasma response that was trained on the Gspert code. This was developed for simulation purposes but could also be useful in real-time operation. In most current tokamak shape control algorithms, feedback gains are calculated offline based on a single reference linearization, and these parameters are used for the entire discharge and across discharges. Using a NN, the equilibrium-dependent response predictions could be served rapidly ($< 1\text{ms}$) throughout the shot as inputs to the control system. Another possible application is in Bayesian-based data analysis in which inference relies on being able to model parameter or diagnostic responses, see e.g. [29, 30].

The rest of this paper is divided as follows. Section 2 introduces Eqnet including the data structure, model architecture, prediction results, and a simple application problem of using Eqnet to design a novel equilibrium. Section 3 describes Pertnet, including the nonrigid plasma response model and relevant background, NN architecture, and performance results.

2. Eqnet

2.1. Problem statement

The goal of this neural net is to identify the plasma equilibrium $\psi(R, Z)$ which is the solution to the free-boundary Grad-Shafranov equation [31, 32]:

$$\begin{aligned} \Delta^* \psi &= -\mu_0 R J_\phi \\ J_\phi &= J_\phi^{pla} + J_\phi^{ext} \\ J_\phi^{pla} &= R P'(\psi) + \frac{F F'(\psi)}{\mu_0 R} \end{aligned} \quad (1)$$

Here ψ is the poloidal flux, J_ϕ is the toroidal current density, $P(\psi)$ is the pressure profile and $F(\psi) := R B_\phi$ is related to the poloidal current. J_ϕ^{ext} is the current density in the shaping coils and surrounding vacuum vessel structures, and serves as a boundary condition for the free-boundary problem. Analytical solutions are known for only a limited number of cases and in general eq. (1) must be solved numerically in an iterative process.

2.2. Data inputs and outputs

The ground truth training data is composed of equilibria generated from the EFIT01 reconstruction algorithm [33, 34] during the 2015-2016 NSTX-U campaign. EFIT01 is a magnetics-only equilibrium reconstruction code which is run automatically after each shot and thus offers a sizeable database of samples (~ 25000 equilibria, spaced 5-10ms apart, from 220 shots). One limitation of magnetics-only reconstructions is that the pressure and current profiles are not well-constrained. On NSTX-U there does exist a small number of discharges for which kinetic equilibria exist (where pressure and current are constrained by Thomson and MSE diagnostic data). However, the EFIT01 reconstruction is generally considered to have high accuracy in fitting the boundary which makes it sufficient for this use-case, and is beneficial due to the higher number of samples.

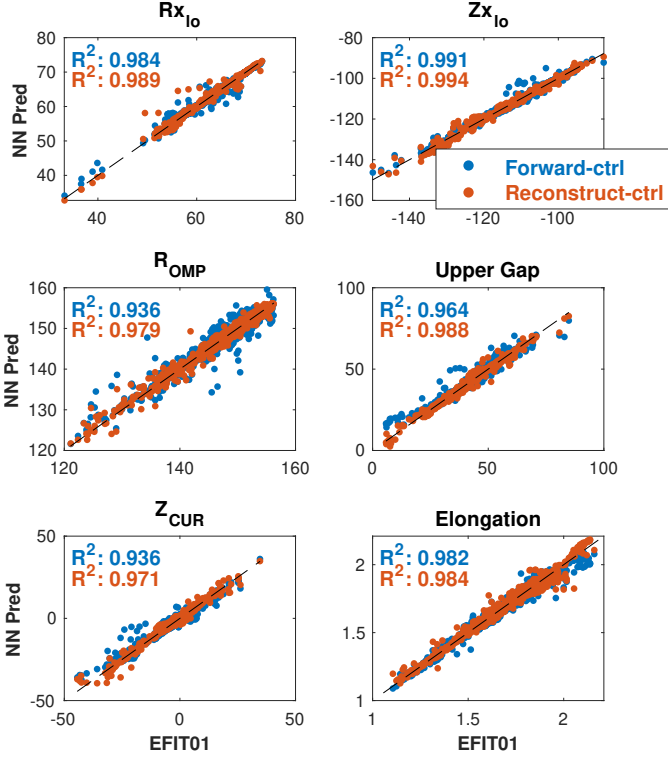


Figure 2: Regression plots of the Eqnet predictions vs EFIT01-measured parameters including: lower x-point position (Rx_{lo} , Zx_{lo}), plasma outer midplane radius R_{OMP} , upper control segment gap (see fig. 6), vertical position of the current centroid Z_{curr} , and plasma elongation. The reconstruction mode performs slightly better than forward mode as determined by R^2 coefficient.

As mentioned, the data inputs and outputs vary depending on the mode of operation. In the forward mode, the NN maps the coil currents, vacuum vessel currents, P' and FF' profiles to the equilibrium flux map. This mode is useful for simulations and optimizing coil current trajectories, since most of these data inputs are readily available from the shape control model (described in more detail in section 3). The shape control model integrates a state vector \mathbf{I} consisting of the plasma, coil, and vessel currents and thus all the current sources are available as inputs at each time step. Often, additional states β_p and l_i are included to track information about the pressure and current (l_i corresponds with the peaked-ness of the plasma current profile). These 2 scalars are almost information-equivalent to knowing the EFIT01 P' and FF' profiles, which by design consist of 1 and 3 basis functions respectively. (We train with the P' and FF' profiles instead of β_p, l_i for flexibility in use cases, since eq. (1) is the standard formulation).

The output of the model is the equilibrium flux values at all grid locations ψ_g , although for better data compression, the NN actually outputs only the plasma flux ψ_g^{pla} . The total flux is the sum of the plasma flux and flux from the external sources.

$$\begin{aligned}\psi_g &= \psi_g^{pla} + \psi_g^{ext} \\ \psi_g^{ext} &= M_{gc}I_c + M_{gv}I_v\end{aligned}\quad (2)$$

Here, M_{gc} and M_{gv} are the mutual inductance matrices between each grid point and the coil and vessel elements respectively, and I_c and I_v are the currents in the coil and vessel elements. The advantage of predicting the plasma flux ψ_g^{pla} is that it has less spatial variation than the total flux leading to better principal component analysis (PCA) data compression and higher accuracy in the final solution. Since all the quantities that constitute ψ_g^{ext} are known, there is no disadvantage to only predicting ψ_g^{pla} .

The reconstruction modes use diagnostics as inputs for estimating the equilibrium, functioning as an alternative version of EFIT. One potential application is to use the NN as a real-time EFIT01 reconstruction instead of the rt-EFIT algorithm [35], as has been proposed for KSTAR [23], since it is known that EFIT01 has better reconstruction accuracy than rtEFIT. However, this type of NN-solver is likely most applicable on smaller machines that do not already have real-time reconstruction algorithms. We train this model using 75 B-probes, 55 flux loops, and 35 vessel current signals and report strong accuracy in the reconstruction, slightly outperforming the forward mode (fig. 2).

The control-oriented modes do not predict the flux but instead predict parameters that are normally derived from the equilibrium. These include: the plasma minor and major radius, elongation, gap sizes of several control segments, positions of the upper and lower x-points, and position of the current centroid. The advantage of this mode is that it bypasses computational steps such locating the touch-point/x-point and tracing the boundary. A shape controller can provide feedback based directly on the NN outputs. A potential downside to this mode is that the outputs are pre-determined, offering less flexibility. If, for example, the position of the shape control segments are adjusted, the NN would have to be retrained with the new control segments.

2.3. Data processing

The dataset is first randomly divided 80-10-10 by shot number into training, validation and testing sets. We divide the dataset by shot number instead of by sample, since adjacent time slices are highly correlated, which could lead to an overestimation of the NN's capability. Each of the target and predictor variables is dimensionally reduced by performing principal component analysis (PCA) on the training set. The number of components kept is selected to achieve 99.5% captured variance, and is summarized for each variable in fig. 3. It should be noted that we do not perform any selection process for including samples as has been done in some previous NN solvers, such as restricting to the flattop portion of the discharge. We include all available samples ranging from t=30ms near the end of

breakdown phase and concluding at shot termination (end of rampdown, disruption, and/or loss of control). Indeed, a sizeable fraction of shots terminate off-normal ($> 30\%$ terminate within 0.6s, while the target pulse length is generally 1–2s) which is a significant contributor to the range and variance in the data, and important for learning.

In order to adequately learn non-flattop equilibria, one step that proved to be necessary for good performance was performing a PCA “merging” procedure on the target variable ψ_g^{pla} . This was done by separating the dataset into rampup, flattop, and rampdown/pre-disruption phases of the discharge, performing PCA on each of these phases separately, and combining the PCA components together to form a single basis. The motivation is that the flattop phase tends to be over-represented because I_p is constant and the flux surfaces and plasma position are mostly constant. In contrast, much of the important variation occurs during rampup and rampdown/pre-disruption. Naively using PCA on the combined data did not represent the rampup or rampdown equilibria well, as determined by visual inspection of the projected flux surfaces. This problem is not fixed by oversampling the rampup and rampdown equilibria, likely because these samples have lower I_p and therefore lower magnitude of ψ_g^{pla} so they still do not sufficiently contribute to the variance in the data matrix.

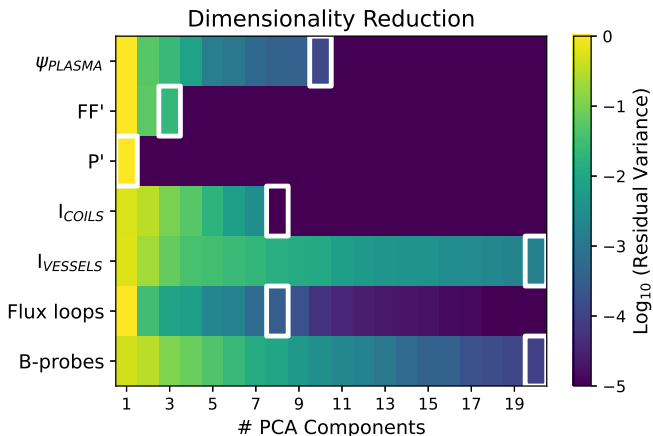


Figure 3: Dimensionality reduction of the Eqnet dataset using Principal Component Analysis (PCA). The outlined boxes indicate 99.5% captured variance and the number of components used for each variable.

The PCA-merging step is performed as follows: suppose we have a data matrix X of dimensions $n_{features} \times n_{samples}$ with sample mean μ , and that we have performed PCA on X and have a set of principal components U and coefficients W . We recall that the data matrix can be projected from the components and coefficients as

$$X = UW + \mu \quad (3)$$

Thus for two (truncated) PCA projections $X_1 = U_1 W_1 + \mu_1$ and $X_2 = U_2 W_2 + \mu_2$, the combined projections $[X_1 \ X_2]$ is within the span of the combined components and means

$\bar{U} := [U_1 \ U_2 \ \mu_1 \ \mu_2]$. Thus we can write

$$[X_1 \ X_2] = \underbrace{[U_1 \ U_2 \ \mu_1 \ \mu_2]}_{\bar{U}} \bar{W} \quad (4)$$

for some set of weights \bar{W} , or a version with nonzero mean which is in the same PCA-like form as eq. (3).

$$[X_1 \ X_2] = \underbrace{[U_1 \ U_2 \ \mu_1 \ \mu_2]}_{\bar{U}} \bar{W} + \mu^* \quad (5)$$

$$\mu^* = (\mu_1 + \mu_2)/2$$

Equation (5) is not a valid PCA projection because the columns of \bar{U} are not orthogonal, but we can obtain a set of orthogonal components U^* by performing, for example, a singular value decomposition of \bar{U} . The merged coefficients are then $W^* = U^{*T}([X_1 \ X_2] - \mu^*)$. This simple preprocessing step proved to be sufficient for compressing data across a wide range of samples. The final result compresses the ψ_g^{pla} grid of size $[65 \times 65]$ to just 10 PCA coefficients.

Figure 3 summarizes data compression results for the various inputs and outputs. For the flux values, significant dimensionality reduction is achieved. As mentioned, the P' and FF' profiles consist of 1 and 3 basis functions respectively, which is captured by this mode decomposition. The highest dimensional inputs are related to the vessel currents and B-probe diagnostics. After dimensionality reduction, we normalize the inputs to have zero mean and unit variance, to arrive at the neural network inputs. The standardization and PCA decompositions are then inverted to map neural network outputs to physical outputs.

2.4. Model architecture and hyperparameter tuning

The model architecture including data processing steps is shown in fig. 4. The core of model is composed of an ensemble of fully-connected artificial neural nets (ANNs) and was created and trained in PyTorch with the Adam optimizer. Each ensemble member is trained on 90% of the training data before averaging the predictions.

The network hyperparameters are chosen by performing scans of number of hidden layers, hidden layer size, dropout fraction, optimizer learn rate, batch size, and non-linearity activation function. Results of this procedure are shown in fig. 5. The hyperparameter landscape appears fairly convex, making it straightforward to identify a suitable parameter combination. We note that the NN tends to perform better with larger network sizes (depth and breadth), zero dropout, and small batch sizes. Though circumstantial this is consistent with some characteristics of the underlying Grad-Shafranov model such as its expressiveness (larger network sizes) and deterministic nature (zero dropout, learning from small batches). We also note a jump in performance when using the ELU activation function as opposed to the standard ReLU.

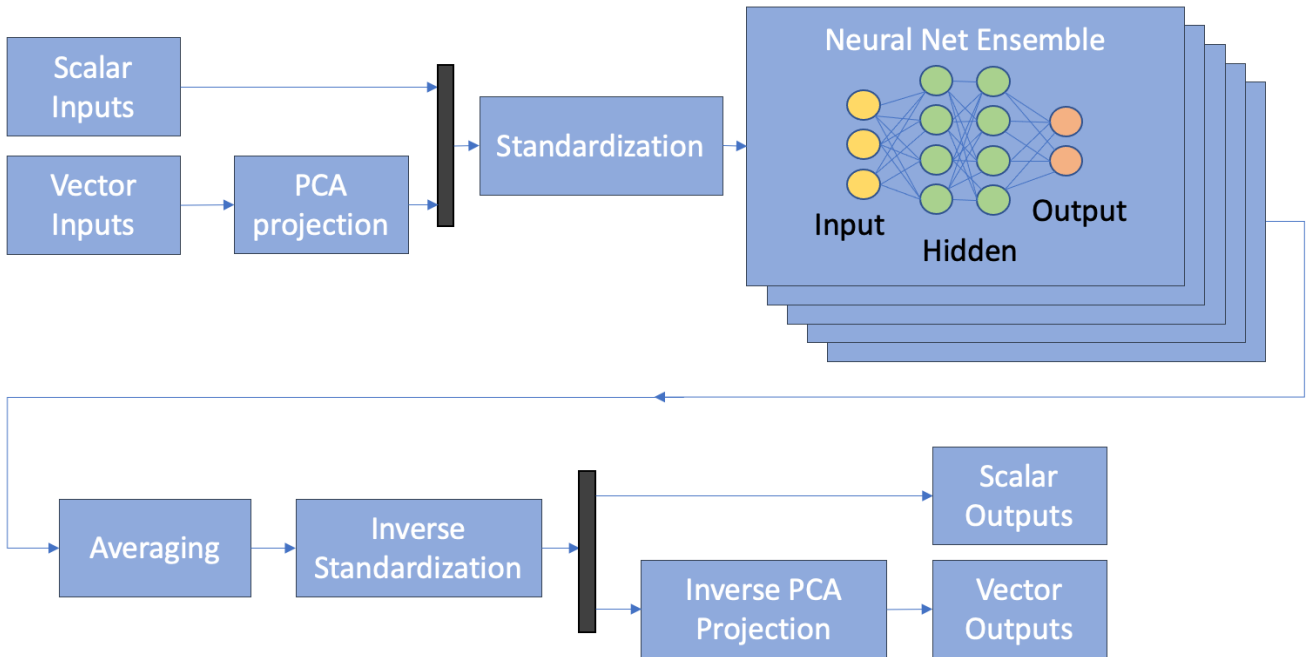


Figure 4: Model architecture for Eqnet and Pertnet including data processing steps. The core of the model is an ensemble of fully-connected networks.

2.5. Performance

Figure 6 shows some representative results for NN flux surface predictions (forward-mode) taken from the test dataset. Also depicted are the x-points, magnetic axis, and control segments used in computing the upper and lower gap. The 4 samples shown represent different categories of equilibrium shapes produced from a limited equilibrium during rampup, upper-single null (USN) diverted during rampup, lower single-null (LSN) during flattop, and a LSN during loss-of-control from a shot that terminated early. The limited and LSN-flattop equilibria are nearly exact and indistinguishable by eye at this scale. These are the 2 most common shapes in the dataset. One can notice some small differences in the boundary for the USN and loss-of-control sample. This suggests, that for these less-represented samples, there is room for improvement either by obtaining more experimental data in the future or supplementing with synthetic equilibria. These samples also tended to occur during highly dynamic periods of the plasma evolution, for example, this USN was produced accidentally during a limited-diverted transition and is accompanied by vertical oscillations.

A regression test of shaping parameters is shown in fig. 2 for the control-oriented NNs. We observe that the reconstruction mode outperforms the forward mode slightly in all variables as measured by the R^2 coefficient. ($R^2 = 1$ is perfect prediction) A possible explanation is that the reconstruction mode has significantly more NN inputs to learn from, including highly localized information from the diagnostics. The hardest variables to predict are the outer

midplane radius and current centroid position with R^2 values 0.936/0.979 and 0.936/0.971. As another quantitative measure of accuracy we note the root-mean-square error (RMSE) for the lower x-point is (forward/reconstruction) $R_{x,lo} = 6.6/5.6\text{mm}$, $Z_{x,lo} = 8.4/7.5\text{mm}$ and for the current centroid $Z_{curr} = 1.4/0.9\text{cm}$, $R_{curr} = 1.1/0.9\text{cm}$. The median error is roughly 50% the RMSE in all cases. While the large majority of samples lie close to the regression line, it is true that some scattered samples have larger deviations of multiple cm.

While errors of multiple cm is high for shape control, the timetrace predictions shown in fig. 7 give some qualifying insight into when these occur. From the R_{OMP} and Z_{CUR} plots we observe multiple spikes in the traces and errors early on, especially within the first few hundred ms. For Z_{CUR} the early errors are also more benign since they occur at low I_p . Z_{CUR} is most important for vertical control, but the applied feedback is proportional to $Z_{CUR}I_p$ [36]. These dynamic features are representative of the NSTX-U campaign and is in part due to the control difficulties of highly-elongated, unstable plasma, and short-pulse (vessel effects become important), machine, as well as EFIT01 reconstruction inaccuracy at very low I_p . The multi-cm error differences generally occur from over-predicting or under-predicting fast transients which occur during these dynamic periods. In fact, for errors $\geq 3\text{cm}$, 68% of bad samples occur during the first or last 100ms of the shot, and 100% within the first or last 200ms.

The timetraces in fig. 7 includes predictions from the forward mode, where shaping parameters have been de-

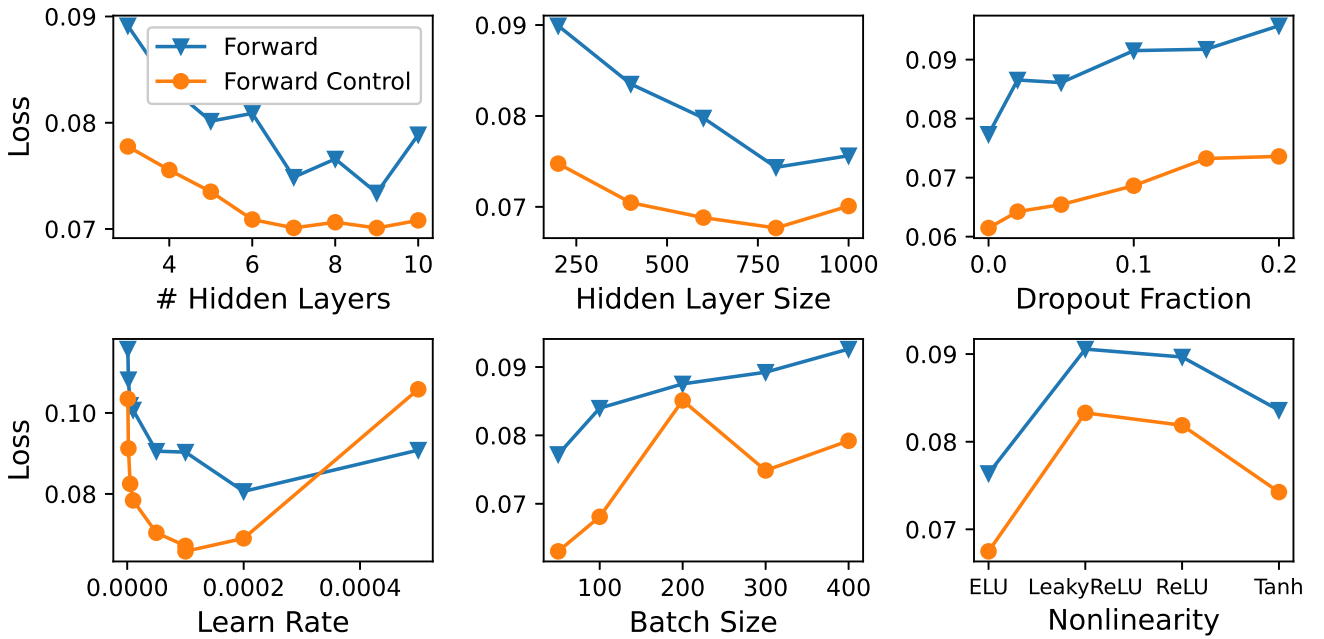


Figure 5: Hyperparameter grid scans used to identify the best performing Eqnet model. The loss value is computed using the validation dataset. The landscape is fairly convex making it straightforward to identify good parameter combinations.

rived from the flux surfaces, as well as the direct prediction of the parameters. Both sets of NN predictions match each other closely and deviate from EFIT01 in roughly the same way, indicating that they are learning equivalent representations of the equilibria. Neither mode is obviously superior to the other, so the only tradeoff is in terms of the desired output type, with flux surface prediction being the more flexible option.

2.6. Design Application

As a simple application task we attempt to solve an inverse equilibrium design problem using the NN. The design problem is: given a target shape, what are the coil currents that will transform an equilibrium into that shape. Notationally, we have target shape \mathbf{y} and the neural net is a map from inputs \mathbf{x} to an equilibrium $f(\mathbf{x})$. (We restrict to only modifying coil currents, not all of the network inputs.) The design procedure is carried out by using the Matlab function `fminsearch`, which is a standard optimization algorithm based on the Nelder-Mead method. At each iteration, the search makes a call to the NN (which evaluates $f(\mathbf{x})$) and adjusts the inputs to minimize the cost function $J := (f(\mathbf{x}) - \mathbf{y})^2$.

The target shape is obtained by beginning with a LSN diverted equilibrium and increasing the elongation from 1.65 to 1.95. The target boundary also has a smaller minor radius 54cm vs 58cm and larger inner and outer gaps. The initial, target, and final shapes are shown in fig. 9, and coil currents in fig. 8. Note that the boundary “final” boundary is not the NN-prediction (which exactly matches the target), but the result of a standard free-boundary cal-

culation using the NN-designed coil currents. The equilibrium produced by the NN is indeed much closer to the target, with some small differences in the boundary at the lower and upper. Given that this is a novel equilibrium for the NN, which has not seen this exact equilibrium before and was not generated via EFIT, we expect this gives a reasonable estimate of generalization error. This level is also acceptable for feedforward planning applications, since feedback control can correct for small errors.

3. Pertnet

“Pertnet” is a neural network we have designed to predict the nonrigid plasma response, which is a term related to the Grad-Shafranov equation that arises in the development of the shape control model. This section includes some background context on the shape control model and plasma response. For further detail on shape control, we refer readers to the review paper by Ambrosino and Albanese [37]. The nonrigid plasma response describes how the plasma current shifts and redistributes in response to changes in the currents of surrounding conductors. The response can be written in units of current or units of flux which are related by the grid mutual inductance:

$$\frac{\partial \psi_i^{pla}}{\partial I_i} = M_{gg} \frac{\partial I_g^{pla}}{\partial I_i} \quad (6)$$

Here, ψ_g^{pla} is the grid flux due to plasma currents, I_g^{pla} is the plasma current distribution, and M_{gg} is the mutual inductance matrix for the grid. We use the “pla” superscript to distinguish flux that is due to plasma sources,

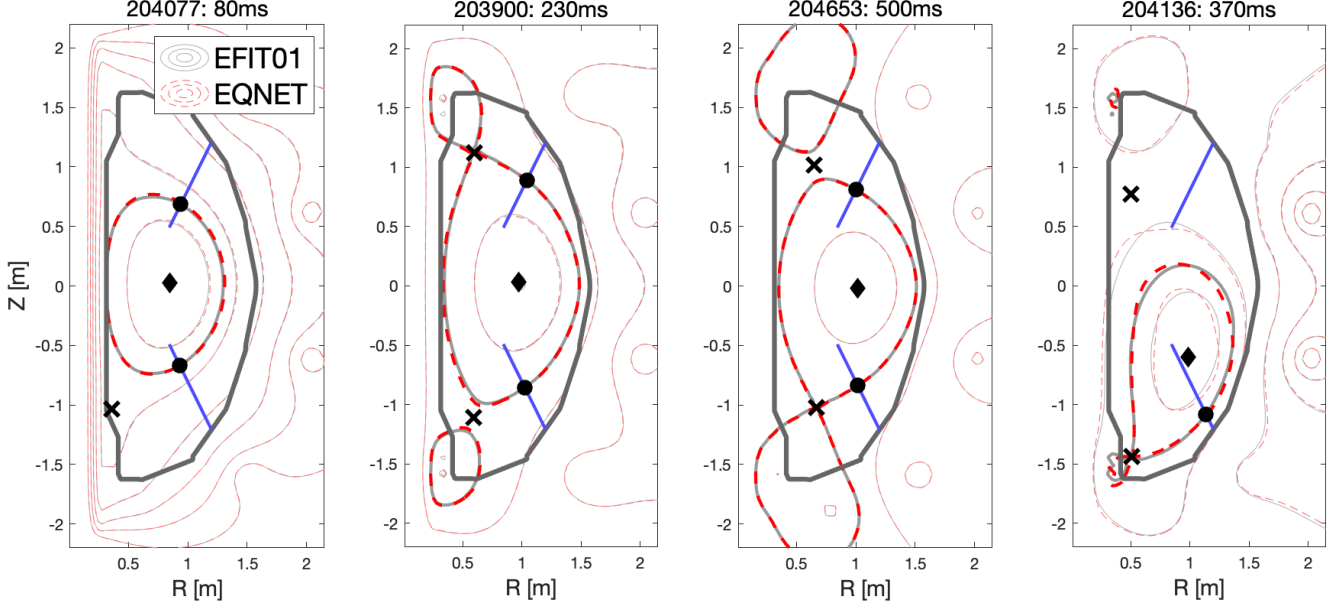


Figure 6: Equilibrium flux surfaces for several test shots as determined by EFIT01 and the Eqnet neural network. The boundary contour is shown in bold. Also shown are control segments (blue), magnetic axis (black diamond), and x-points.

since the total flux at any point is due to both plasma and external sources. The physical interpretation is that when the current in an external conductor is perturbed, this changes the background magnetic field. Since the plasma is carrying current it experiences a Lorentz force that causes it to shift back into equilibrium. We rely on the Gspert code [25] to obtain the plasma response, which is based on a linearization to the Grad-Shafranov equation. In addition to obtaining the response due to current changes, it is often useful to obtain the response due to changes in global parameters such as β_p and l_i . These are included in the Pertnet predictions, although not explicitly discussed here.

The plasma response arises in several places in the shape control model. For example, the model often begins by writing a circuit equation for all the conducting elements within the tokamak:

$$\begin{aligned}
 v_i &= R_i I_i + \dot{\psi}_i \\
 &= R_i I_i + M_{ij} \dot{I}_j + \frac{\partial \psi_i^{pla}}{\partial I_j} \dot{I}_j \\
 &= R_i I_i + M_{ij} \dot{I}_j + M_{ig} \frac{\partial I_g^{pla}}{\partial I_j} \dot{I}_j
 \end{aligned} \tag{7}$$

where v_i is the applied voltage from external power supplies, R_i is the resistance of each element. We see that the plasma response contributes to the flux change at conductors and must be accounted for when modeling current evolution. Additionally, this term is needed for modelling how various feedback parameters (x-points, current cen-

teroid) change with respect to the inputs. Consider some inputs x that define the equilibrium (x includes the coil currents), and some shaping parameters y that are derived from the equilibrium flux. This relation is

$$y = f(\psi(x)) \tag{8}$$

$f(\cdot)$ is the mapping from equilibrium to parameters, and $\psi(\cdot)$ is the map from inputs to equilibrium. By the chain rule, in order to see how the inputs affect the shape parameters we need access to the plasma response.

$$\frac{\partial y}{\partial x} = \frac{\partial f}{\partial \psi_g} \left(\frac{\partial \psi_g^{ext}}{\partial x} + \frac{\partial \psi_g^{pla}}{\partial x} \right) \tag{9}$$

We train 2 versions of the Pertnet model – a standard flux mode that calculates the flux response $\frac{\partial \psi_g^{pla}}{\partial x}$ and a control-oriented mode that directly estimates the parameter responses $\frac{\partial y}{\partial x}$. To illustrate this mapping from flux response to parameter response via eq. (9), we show the derivation for 3 parameters (current centroid response, x-point response, and vertical growth rate) which are the main parameters predicted by the Pertnet control mode:

3.0.1. Current centroid response

The current centroid position is the current-weighted average of each coordinate over the plasma domain Ω :

$$Z_{cur} = \frac{1}{I_p} \sum_{\Omega} Z_g I_g \tag{10}$$

Applying eq. (9) and eq. (6) gives

204125

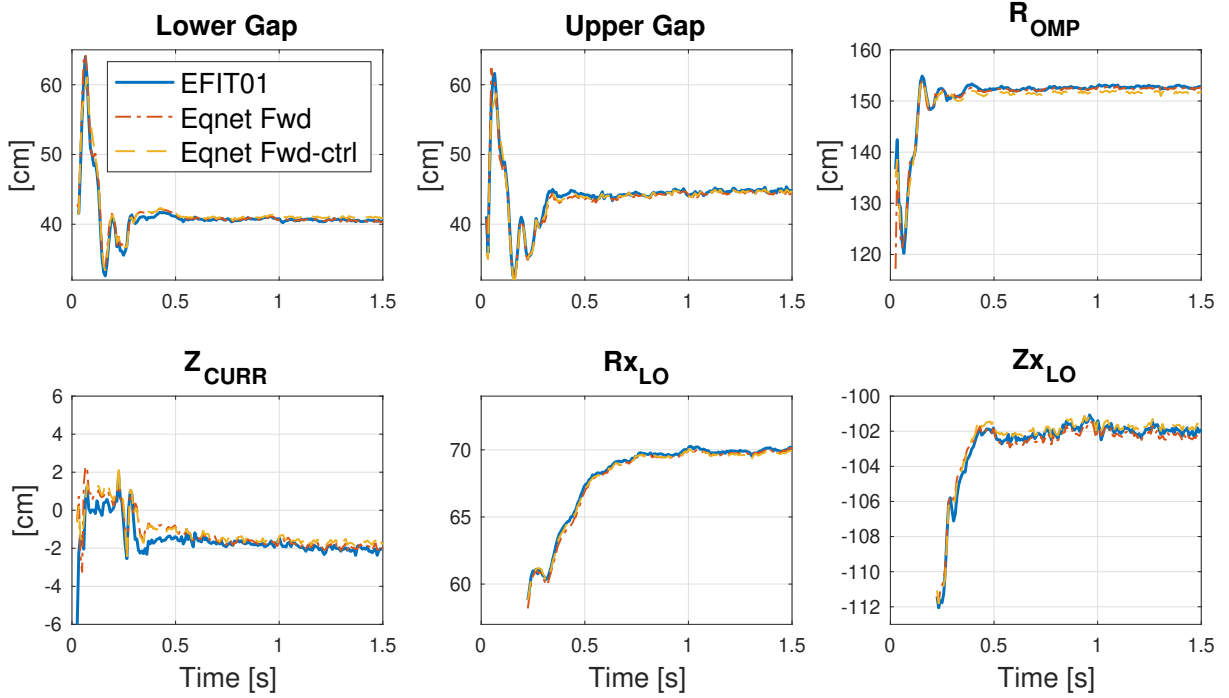


Figure 7: Time traces of several geometric quantities for test dataset shot 204125, as measured by EFIT01 and predicted by Eqnet. The lower and upper gaps are the intersection of the plasma boundary with the control segments as shown in fig. 6.

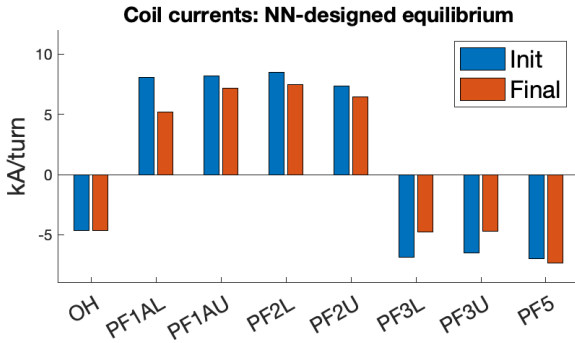


Figure 8: Coil currents designed by with fminsearch + Eqnet in order to construct an elongated equilibrium.

$$\frac{\partial Z_{cur}}{\partial x} = \frac{1}{I_p} \sum_{\Omega} Z_g \left(M_{gg}^{-1} \frac{\partial \psi_{g,pla}}{\partial x} \right) \quad (11)$$

3.0.2. X-point response

The x-point is the location at which the flux gradient is equal to zero, so finding the x-point is equivalent to finding the root of the equation $F(\mathbf{s}) = [\psi_r(\mathbf{s}) \ \psi_z(\mathbf{s})]^T$. Using Newton's method with the Jacobian of F defined J_F , one could find the root by successively applying updates as

$$\Delta \mathbf{s} = -J_F(\mathbf{s})^{-1} F(\mathbf{s}) \quad (12)$$

If we have already converged to an x-point, but then

apply a perturbation to the flux, the response of the x-point is

$$\frac{\partial(r_x, z_x)}{\partial x} = \frac{\partial \Delta \mathbf{s}}{\partial x} = -J_F(\mathbf{s})^{-1} \begin{bmatrix} \frac{\partial \psi_r}{\partial x} \\ \frac{\partial \psi_z}{\partial x} \end{bmatrix} \quad (13)$$

which depends explicitly on the plasma response via the last terms since

$$\frac{\partial \psi_r}{\partial x} = \frac{\partial}{\partial r} \left(\frac{\partial \psi^{ext}}{\partial x} + \frac{\partial \psi^{pla}}{\partial x} \right) \quad (14)$$

3.0.3. Vertical growth rate

The vertical growth rate is an instability that can be related to the evolution of currents in conducting structures. Defining the response term in eq. (7) as $X_{ij} := \frac{\partial \psi_i^{pla}}{\partial I_j}$, this equation can be rewritten in matrix form as

$$\mathbf{v} = \mathbf{R}\mathbf{I} + (\mathbf{M} + \mathbf{X})\dot{\mathbf{I}} \quad (15)$$

or equivalently

$$\begin{aligned} \dot{\mathbf{I}} &= \mathbf{A}\mathbf{I} + \mathbf{B}\mathbf{v} \\ \mathbf{A} &:= -(\mathbf{M} + \mathbf{X})^{-1}\mathbf{R} \\ \mathbf{B} &:= (\mathbf{M} + \mathbf{X})^{-1} \end{aligned} \quad (16)$$

which is the standard form of the shape control state space model. The vertical growth rate is taken as the

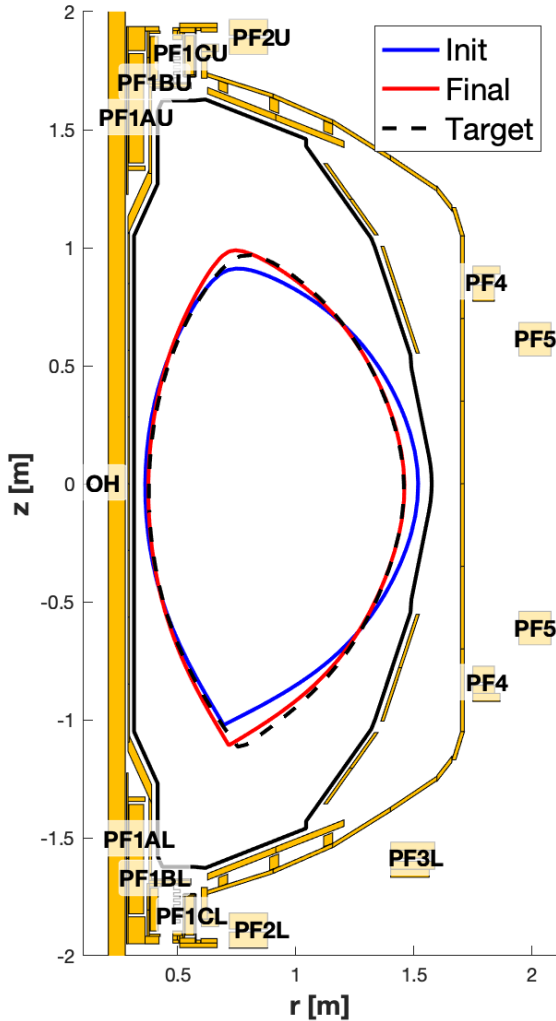


Figure 9: Equilibrium designed with `fminsearch` + `Eqnet`, by adjusting the coil currents in order to match the target boundary. The target shape is an elongated $\kappa = 1.95$ LSN equilibrium.

largest unstable eigenvalue of the \mathbf{A} matrix.

$$\gamma = \max(\text{real}(\text{eig}(\mathbf{A}))) \quad (17)$$

3.1. Data Inputs and Outputs

Similar to `Eqnet`, we train 2 versions of the `Pertnet` model – a “standard” flux mode that calculates the flux response $\frac{\partial \psi_q^{pla}}{\partial x}$ and a “control” mode that predicts the parameter responses $\frac{\partial y}{\partial x}$. The standard mode is more general in that all aspects of the shape control model can be derived from it, albeit with more computational effort. On the other hand, control mode skips some computational steps in finding the shaping parameter response directly. This would make it useful for experiments in providing fast estimates to the shape controller. A potential downside is

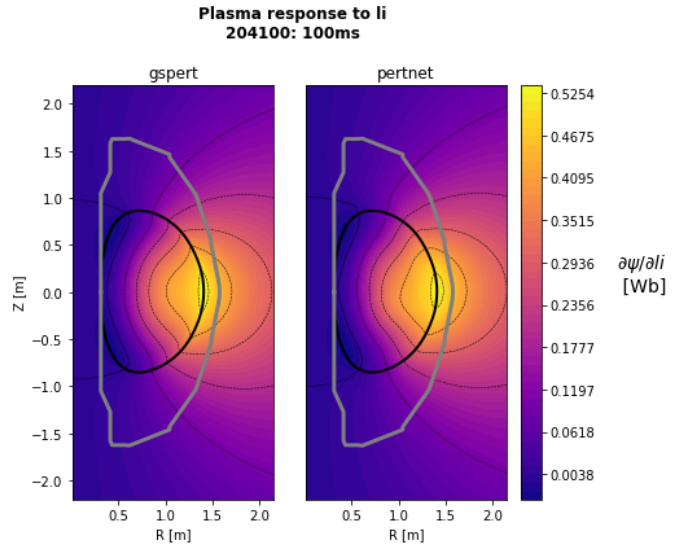


Figure 10: Comparison of the plasma response to an l_i perturbation as calculated by the `Gspert` code and `pertnet` neural network approximator. The plasma boundary is overlaid in black.

that if the desired outputs are modified then the NN requires retraining. Additionally, the control mode does not predict all aspects of the shape control model, such as what the full \mathbf{X} matrix is.

For both modes, the inputs are a complete description of the equilibrium. We assume more inputs here than we did for `Eqnet` because we are linearizing around the current equilibrium and can thus assume access to it, either via a NN prediction or reconstruction algorithm. The inputs include: $\psi(r, z)$ as calculated by `EFIT01`, the `EFIT01` pressure $P'(\psi)$ and $FF'(\psi)$ profiles, current distribution J_ϕ , coil and vessel currents, I_p , coordinates of the boundary contour, ψ at the magnetic axis and boundary, and the (R, Z) position of the magnetic axis, x-points, and current centroid.

For the standard mode, the output is the flux response on the grid. Note that from eq. (6) we could predict in units of flux or units of currents. For the NN, it is advantageous to predict in flux units. This is because the current response can contain highly localized information about the current variation in nearby grid cells. By contrast the flux response has less spatial variation and has better data compression. In other words, the grid mutual inductance M_{gg} acts like a smoothing or averaging filter when transforming from current to flux.

3.2. Architecture and hyperparameter tuning

We use the same ~ 25000 equilibrium samples and 80-10-10 dataset split as in `Eqnet`. For each sample, we run `Gspert` to find the plasma response to the 8 active PF coils, 40 vessel circuits, I_p , β_p , and l_i . For the standard mode, we train an individual NN to predict the response of each quantity. This performs better than predicting the flux response to all inputs simultaneously, which does

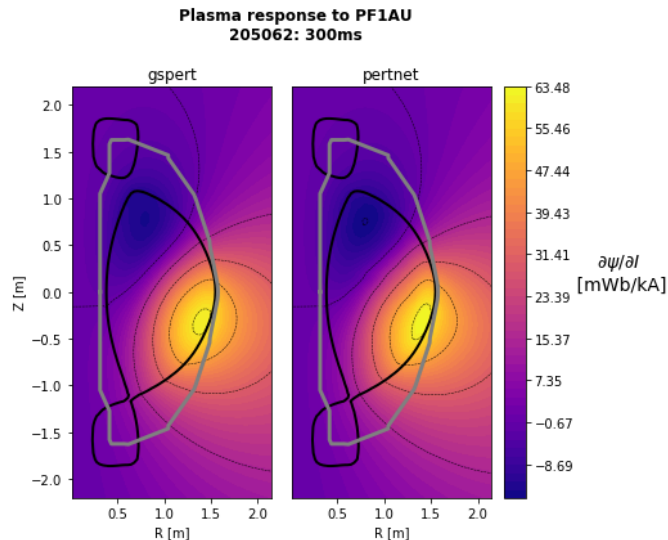


Figure 11: Comparison of the plasma response to a PF1AU current perturbation as calculated by the Gspert code and pertnet neural network approximator. The plasma boundary is overlaid in black.

not dimensionally reduce very well, since each response quantity can vary significantly in magnitude. Additionally, the computational burden of multiple NN's can be eased by parallelization during training and inference. For the control mode, which predicts responses of individual parameters that are of much lower dimension than the flux response, it was found that a single NN was sufficient.

Principal component analysis is used to compress all the inputs and outputs, choosing the number of components to capture 99.5% variance, with results of this procedure shown in fig. 15. Only some of the response quantities are plotted. Note that the equilibrium currents J_ϕ has a much larger representation than the flux ψ , again indicating that the flux is generally smoother than the current. All response variables have the similar order of magnitude (~ 10 components. Some variables, such as the ohmic (OH) coil have expectedly higher variation. The OH coil spans the entire vertical length of NSTX-U, and thus can interact with the plasma from multiple angles depending on plasma position. After PCA, the coefficients are then normalized to zero mean and unit variance. The full architecture of the model is identical to Eqnet and shown in fig. 4.

Training is performed in Pytorch with the Adam optimizer. Hyperparameters are selected by performing grid scans over the various model parameters such as size and depth, with results shown in fig. 16. Early on, it was observed visually that using the L1 loss (absolute error) function performed better than the standard L2 loss (sum of squares). This is theorized to be a result of noise and outliers in the dataset. In particular, a small fraction of samples were observed to have spurious results due to running Gspert automatically on all 25k+ equilibria. These include errors such as not converging fully to features of

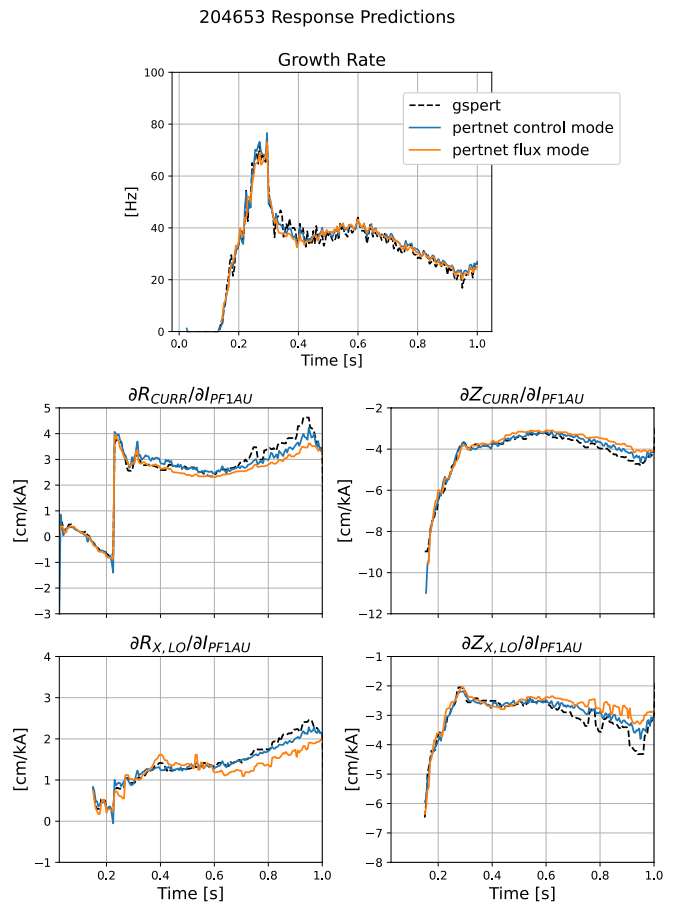


Figure 12: Predictions of the plasma response for several parameters (growth rate, current centroid response to PF1AU, and x-point position response to PF1AU) as calculated by Gspert and versions of Pertnet. The Pertnet control mode directly predicts these parameters, while the pertnet flux mode predicts the flux response which maps to the parameter responses.

interest, or not identifying the boundary correctly in a situation with multiple x-points and touch points. An attempt was made to perform automated filtering of the outputs, but manual inspection of all results was not performed. In addition, the samples are theorized to have a lot of noise due to the inherent noise associated with taking derivatives. Since L2 penalizes squared errors, the network was probably learning too much from predictions with large errors that should have been identified as outliers. Another possible indicator of stochasticity is that the performance improves by including 5 – 10% dropout on the network weights during training. The final network is smaller than Eqnet with the standard/control modes having 4/5 layers with hidden layer size 400/800. Note that the hyperparameters differ significantly between the modes because they are actually problems with relatively different structure, since the standard mode has a NN for each flux response, and the control mode is a single NN that predicts all parameter responses.

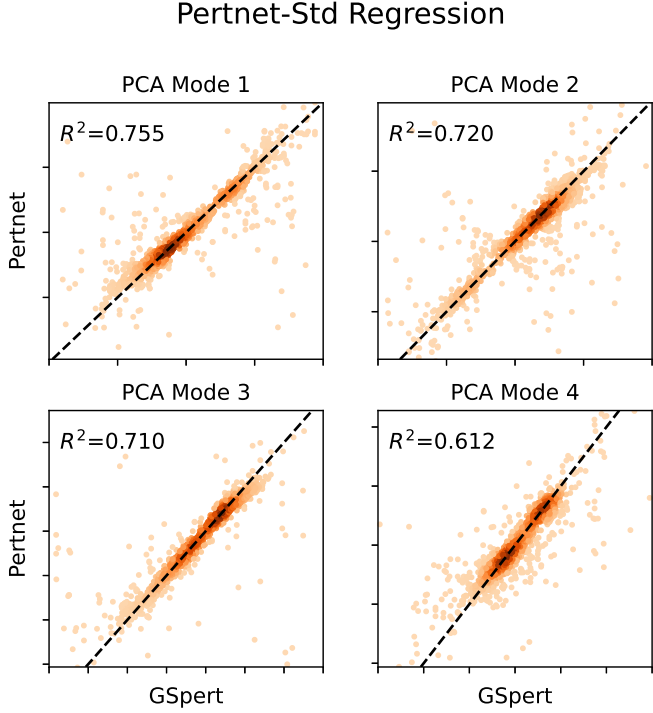


Figure 13: Regression of the Pertnet flux prediction vs calculated values from Gspert. The data shown is the test dataset for the response to PF5. Each plot shows the coefficient of the corresponding PCA mode of the flux response.

3.3. Performance

Performance of the flux response prediction is shown in fig. 13 where we have plotted the NN-predicted PCA coefficient vs the Gspert values, for the first 4 PCA modes. These predictions are for the flux response to PF5 the midplane outboard shaping, for the entire test dataset. The densest clusters lie close to the true values, though there is scatter for individual sample points. As expected, the prediction is most accurate on the first PCA mode ($R^2 = 0.755$) and decreases slightly with each increasing mode number.

Figure 10 and fig. 11 show individual flux responses to two different perturbation sources, l_i and the upper inboard coil PF1AU. The predicted vs actual flux responses are difficult to distinguish by eye, although there are some slight differences. Predictions of the timetraces for parameter responses are plotted in fig. 12 for as single shot 204653. These include the current centroid response, x-point response, and growth rate as obtained by eqs. (11), (13) and (17). Even though the flux response is not trained to predict these parameters, the extracted parameter response is close to the Gspert values. However, if only interested in the parameter response, the control mode outperforms slightly. For example, in the second half of the shot, Gspert estimates that the radial position of the x-point ($R_{X,LO}$) will grow increasingly more sensitive to the PF1AU coil. The control-mode captures this trend, though the standard flux mode does not trend as strongly.

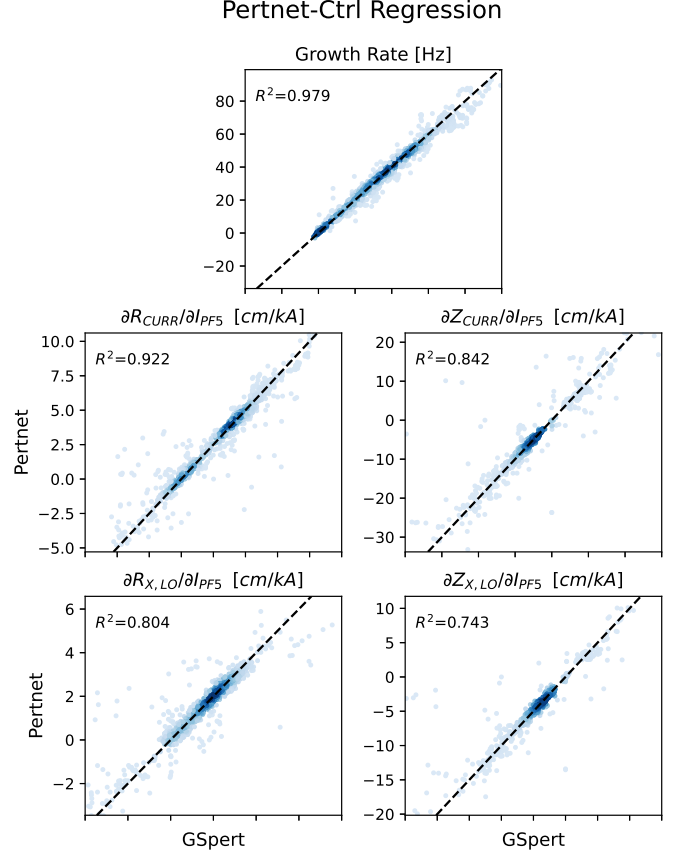


Figure 14: Regression of Pertnet parameter responses vs the Gspert values, based on predictions from Pertnet-control mode.

The growth rate prediction for both models matches Gspert very accurately, which is a nice confirmation of prediction of all the NN models. Note that the growth rate prediction is unlike the other parameters, in that it does not depend on the response to just one input coil, but all the coils simultaneously (via eqs. (16) and (17), since the \mathbf{X} matrix includes effects from all coils). Even if individual flux responses can each have inaccuracies, this is an indicator that the dominant effects upon the coil current dynamics is being captured.

Lastly, fig. 14 shows the performance of Pertnet-control mode for predicting individual parameter responses, in this case to PF5. We note that the individual responses generally have slightly higher correlation coefficients than prediction of the flux modes. While it is not a linear transformation between flux and parameters, this is consistent with the observation on fig. 12 that direct parameter prediction performed slightly better. The most accurate prediction is the growth rate ($R^2 = 0.979$, RMSE = 3.2Hz) while the least accurate is the Z-position of the x-point ($R^2 = 0.698$, RMSE=2.7cm/kA). The median absolute error (MAE) for this parameter is only 0.17cm/kA and much lower than the RMSE, indicating that a smaller number of samples contribute significantly to the error. Again, it turns out that the largest responses and prediction errors

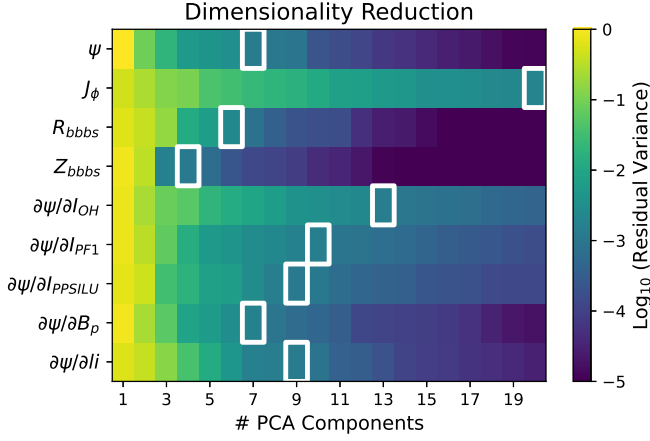


Figure 15: Dimensionality reduction of the Pertnet dataset using Principal Component Analysis (PCA). The outlined boxes indicate 99.5% captured variance and the number of components used for each variable.

are primarily a result of the dynamic periods during ramp-up and loss-of-control (e.g. for the worst 5% of predictions, 88% occur within the first or last 200ms of the shot). This tends to manifest itself worse in the vertical direction than in the radial direction, consistent with the vertical instability effect. Note the scale difference for R-coordinate response vs the Z-coordinate responses, and that the R^2 coefficient for radial responses is higher indicating better predictions for this direction.

4. Conclusion

In this work we have introduced two neural nets for the NSTX-U tokamak, as part of a suite of prediction and simulation tools being developed for optimizing plasma scenarios. The neural nets include Eqnet, a free boundary equilibrium solver, and Pertnet which calculates the non-rigid plasma response. As a simple application, we use Eqnet to design the coil currents for a desired target equilibria, indicating good performance and stability. Both neural nets are trained and tested with different combinations of input and output data. We find that using Eqnet to reconstruct equilibria from magnetic diagnostics gives a small but consistent improvement in accuracy compared to using profile inputs like a traditional free-boundary Grad-Shafranov solver. However the traditional free-boundary solver mode offers some unique advantages and flexibility. We also report strong performance for Pertnet in predicting the plasma response. If only interested in the response of various parameters, it is simpler (fewer NNs to train) and marginally more accurate to predict these directly. However, predicting the full flux response is needed in some situations and can give good estimates of the parameters with additional computational steps.

Acknowledgements

This work was supported by the US Department of Energy Grant under contract numbers DE-AC02-09CH11466 and DE-SC0015878.

References

- [1] A. Jalalvand, et al., Real-time and adaptive reservoir computing with application to profile prediction in fusion plasma, IEEE Transactions on Neural Networks and Learning Systems (2021) 1–12. doi:[10.1109/tnnls.2021.3085504](https://doi.org/10.1109/tnnls.2021.3085504).
- [2] J. Abbate, et al., Data-driven profile prediction for DIII-d, Nuclear Fusion 61 (2021) 046027. doi:[10.1088/1741-4326/abe08d](https://doi.org/10.1088/1741-4326/abe08d).
- [3] M. Boyer, J. Chadwick, Prediction of electron density and pressure profile shapes on NSTX-u using neural networks, Nuclear Fusion 61 (2021) 046024. doi:[10.1088/1741-4326/abe08b](https://doi.org/10.1088/1741-4326/abe08b).
- [4] H. LI, et al., Machine learning of turbulent transport in fusion plasmas with neural network, Plasma Sci. Technol. 23 (2021) 115102. doi:[10.1088/2058-6272/ac15ec](https://doi.org/10.1088/2058-6272/ac15ec).
- [5] P. Gaudio, et al., An alternative approach to the determination of scaling law expressions for the l-h transition in tokamaks utilizing classification tools instead of regression, Plasma Phys. Control. Fusion 56 (2014) 114002. doi:[10.1088/0741-3335/56/11/114002](https://doi.org/10.1088/0741-3335/56/11/114002).
- [6] A. Murari, et al., Machine learning for the identification of scaling laws and dynamical systems directly from data in fusion, Nuclear Instruments and Methods in Physics Research Section A: Accelerators, Spectrometers, Detectors and Associated Equipment 623 (2010) 850–854. doi:[10.1016/j.nima.2010.02.080](https://doi.org/10.1016/j.nima.2010.02.080).
- [7] C. Rea, et al., A real-time machine learning-based disruption predictor in DIII-d, Nucl. Fusion 59 (2019) 096016. doi:[10.1088/1741-4326/ab28bf](https://doi.org/10.1088/1741-4326/ab28bf).
- [8] M. Lungaroni, et al., On the potential of ruled-based machine learning for disruption prediction on JET, Fusion Engineering and Design 130 (2018) 62–68. doi:[10.1016/j.fusengdes.2018.02.087](https://doi.org/10.1016/j.fusengdes.2018.02.087).
- [9] K. Montes, et al., Machine learning for disruption warnings on alcator c-mod, DIII-d, and EAST, Nucl. Fusion 59 (2019) 096015. doi:[10.1088/1741-4326/ab1df4](https://doi.org/10.1088/1741-4326/ab1df4).
- [10] Y. Fu, et al., Machine learning control for disruption and tearing mode avoidance, Physics of Plasmas 27 (2020) 022501. doi:[10.1063/1.5125581](https://doi.org/10.1063/1.5125581).
- [11] A. Pau, et al., A machine learning approach based on generative topographic mapping for disruption prevention and avoidance at JET, Nucl. Fusion 59 (2019) 106017. doi:[10.1088/1741-4326/ab2ea9](https://doi.org/10.1088/1741-4326/ab2ea9).
- [12] J. Kates-Harbeck, et al., Predicting disruptive instabilities in controlled fusion plasmas through deep learning, Nature 568 (2019) 526–531. doi:[10.1038/s41586-019-1116-4](https://doi.org/10.1038/s41586-019-1116-4).
- [13] A. Piccione, et al., Physics-guided machine learning approaches to predict the ideal stability properties of fusion plasmas, Nucl. Fusion 60 (2020) 046033. doi:[10.1088/1741-4326/ab7597](https://doi.org/10.1088/1741-4326/ab7597).
- [14] M. Boyer, et al., Real-time capable modeling of neutral beam injection on NSTX-u using neural networks, Nuclear Fusion 59 (2019) 056008. doi:[10.1088/1741-4326/ab0762](https://doi.org/10.1088/1741-4326/ab0762).
- [15] E. Coccoresse, et al., Identification of noncircular plasma equilibria using a neural network approach, Nuclear Fusion 34 (1994) 1349–1363. doi:[10.1088/0029-5515/34/10/i05](https://doi.org/10.1088/0029-5515/34/10/i05).
- [16] J. Lister, H. Schnurrenberger, Fast non-linear extraction of plasma equilibrium parameters using a neural network mapping, Nuclear Fusion 31 (1991) 1291–1300. doi:[10.1088/0029-5515/31/7/005](https://doi.org/10.1088/0029-5515/31/7/005).
- [17] R. Albanese, et al., Identification of plasma equilibria in ITER from magnetic measurements via functional parameterization and neural networks, Fusion Technology 30 (1996) 219–236. doi:[10.13182/fst96-a30752](https://doi.org/10.13182/fst96-a30752).

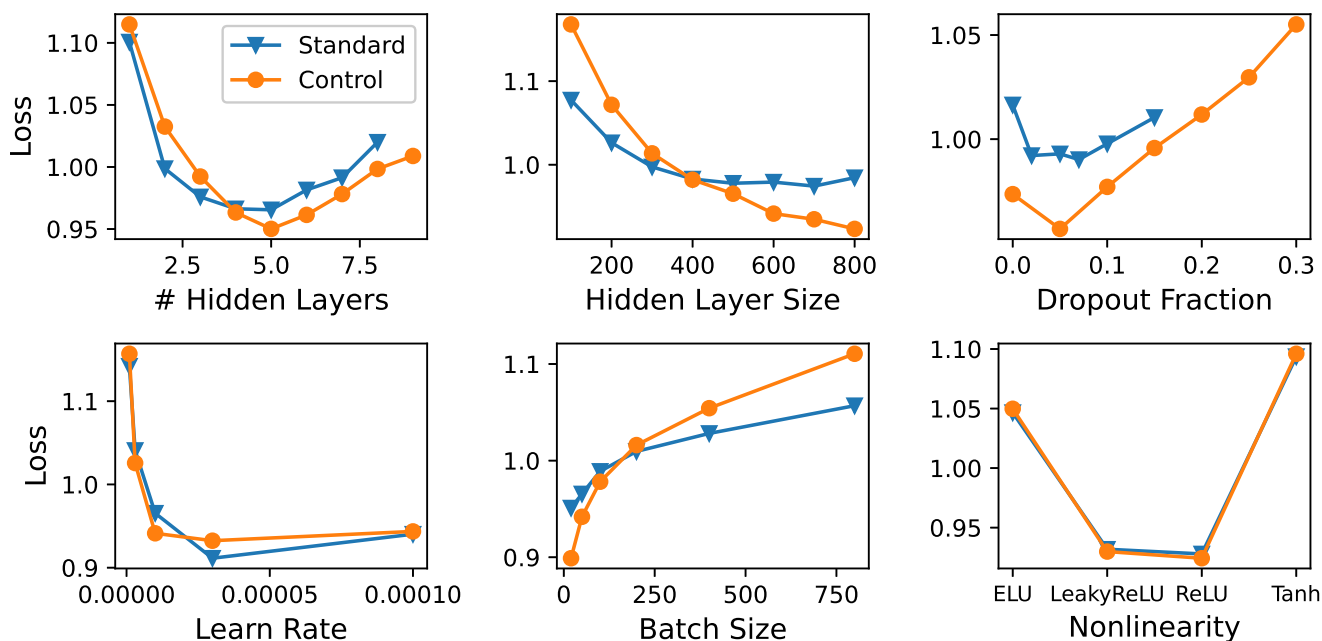


Figure 16: Hyperparameter grid scans used to identify the best performing Pertnet model. The optimal model depends on which Pertnet mode is under consideration, with the control mode favoring larger networks than the standard mode.

- [18] C. M. Bishop, et al., Real-time control of a tokamak plasma using neural networks, *Neural Computation* 7 (1995) 206–217. doi:[10.1162/neco.1995.7.1.206](https://doi.org/10.1162/neco.1995.7.1.206).
- [19] L. Lagin, et al., Application of neural networks for real-time calculations of plasma equilibrium parameters for PBX-M, in: *Fusion Technology 1992*, Elsevier, 1993, pp. 1057–1061. doi:[10.1016/b978-0-444-89995-8.50205-8](https://doi.org/10.1016/b978-0-444-89995-8.50205-8).
- [20] Z.-J. Zhu, et al., Estimation of plasma equilibrium parameters via a neural network approach, *Chinese Physics B* 28 (2019) 125204. doi:[10.1088/1674-1056/ab55d1](https://doi.org/10.1088/1674-1056/ab55d1).
- [21] A. A. Prokhorov, et al., The plasma shape control system in the tokamak with the artificial neural network as a plasma equilibrium reconstruction algorithm, *IFAC-PapersOnLine* 53 (2020) 857–862. doi:[10.1016/j.ifacol.2020.12.843](https://doi.org/10.1016/j.ifacol.2020.12.843).
- [22] B. Wang, et al., Artificial neural networks for data analysis of magnetic measurements on east, *Journal of Fusion Energy* 35 (2015) 390–400. doi:[10.1007/s10894-015-0044-z](https://doi.org/10.1007/s10894-015-0044-z).
- [23] S. Joung, et al., Deep neural network grad-shafranov solver constrained with measured magnetic signals, *Nuclear Fusion* 60 (2019) 016034. doi:[10.1088/1741-4326/ab555f](https://doi.org/10.1088/1741-4326/ab555f).
- [24] B. P. van Milligen, et al., Neural network differential equation and plasma equilibrium solver, *Physical Review Letters* 75 (1995) 3594–3597. doi:[10.1103/physrevlett.75.3594](https://doi.org/10.1103/physrevlett.75.3594).
- [25] A. S. Welander, et al., Nonrigid, linear plasma response model based on perturbed equilibria for axisymmetric tokamak control design, *Fusion Science and Technology* 47 (2005) 763–767. doi:[10.13182/fst05-a778](https://doi.org/10.13182/fst05-a778).
- [26] A. Welander, et al., Closed-loop simulation with grad-shafranov equilibrium evolution for plasma control system development, *Fusion Engineering and Design* 146 (2019) 2361–2365. doi:[10.1016/j.fusengdes.2019.03.191](https://doi.org/10.1016/j.fusengdes.2019.03.191).
- [27] R. Albanese, F. Villone, The linearized CREATE-I plasma response model for the control of current, position and shape in tokamaks, *Nucl. Fusion* 38 (1998) 723–738. doi:[10.1088/0029-5515/38/5/307](https://doi.org/10.1088/0029-5515/38/5/307).
- [28] R. Albanese, et al., CREATE-NLa robust control-oriented free boundary dynamic plasma equilibrium solver, *Fusion Engineering and Design* 96-97 (2015) 664–667. doi:[10.1016/j.fusengdes.2015.06.162](https://doi.org/10.1016/j.fusengdes.2015.06.162).
- [29] J. Svensson, A. Werner, Current tomography for axisymmetric plasmas, *Plasma Physics and Controlled Fusion* 50 (2008) 085002. URL: <https://doi.org/10.1088/0741-3335/50/8/085002>. doi:[10.1088/0741-3335/50/8/085002](https://doi.org/10.1088/0741-3335/50/8/085002).
- [30] G. T. von Nessi, M. J. Hole, A unified method for inference of tokamak equilibria and validation of force-balance models based on bayesian analysis, *Journal of Physics A: Mathematical and Theoretical* 46 (2013) 185501. URL: <https://doi.org/10.1088/1751-8113/46/18/185501>. doi:[10.1088/1751-8113/46/18/185501](https://doi.org/10.1088/1751-8113/46/18/185501).
- [31] H. Grad, H. Rubin, Hydromagnetic equilibria and force-free fields, *Proceedings of the 2nd UN Conf. on the Peaceful Uses of Atomic Energy* 31 (1958) 190.
- [32] V. Shafranov, Plasma equilibrium in a magnetic field, *Reviews of Plasma Physics* (1966) 103.
- [33] L. Lao, et al., Reconstruction of current profile parameters and plasma shapes in tokamaks, *Nuclear Fusion* 25 (1985) 1611–1622. URL: <https://doi.org/10.1088/0029-5515/25/11/007>. doi:[10.1088/0029-5515/25/11/007](https://doi.org/10.1088/0029-5515/25/11/007).
- [34] S. Sabbagh, et al., Equilibrium properties of spherical torus plasmas in NSTX, *Nuclear Fusion* 41 (2001) 1601–1611. URL: <https://doi.org/10.1088/0029-5515/41/11/309>. doi:[10.1088/0029-5515/41/11/309](https://doi.org/10.1088/0029-5515/41/11/309).
- [35] J. R. Ferron, et al., Real time equilibrium reconstruction for control of the discharge in the diii-d tokamak (1997). URL: <https://www.osti.gov/biblio/505400>.
- [36] M. Boyer, et al., Plasma boundary shape control and real-time equilibrium reconstruction on NSTX-u, *Nuclear Fusion* 58 (2018) 036016. doi:[10.1088/1741-4326/aaa4d0](https://doi.org/10.1088/1741-4326/aaa4d0).
- [37] G. Ambrosino, R. Albanese, Magnetic control of plasma current, position, and shape in tokamaks: a survey or modeling and control approaches, *IEEE Control Systems Magazine* 25 (2005) 76–92. doi:[10.1109/MCS.2005.1512797](https://doi.org/10.1109/MCS.2005.1512797).